NOAA Technical Memorandum EDIS 27

GATE RADAR CAPPI DERIVATION FOR THREE-
DIMENSIONAL REFLECTIVITY ANALYSES

Washington, D.C.
July 1979

NOAA TECHNICAL MEMORANDUMS

Environmental Data and Information Service Series

The Environmental Data and Information Service (EDIS) is responsible for storing, retrieving, and publishing data gathered by NOAA and for developing systems to process and present NOAA data in the most useful historical and statistical form. These data, which relate to the solid earth, ocean, atmosphere, and extra-terrestrial space, are the basic input in scientific and engineering studies having broad application in agriculture, commerce, defense, and industry.

The EDIS series of NOAA Technical Memorandums facilitates rapid distribution of studies and reports which may be preliminary in nature and which may be published formally elsewhere at a later date. Publications 1 and 2 are in a former series of Weather Bureau Technical Notes (TN); publications 3 to 17 are in a former series of ESSA Technical Memorandums designated as Environmental Data Service Technical Memorandums (EDSTM). Beginning with 18, publications are now part of the NOAA Technical Memorandum EDIS series and are designated as either EDS or EDIS.

Publications listed below are available from the National Technical Information Service, U.S. Department of Commerce, Sills Bldg., 5285 Port Royal Road, Springfield, VA 22161. Price: Varies for paper copy; $3.00 microfiche. Order by accession number shown in parentheses at end of each entry.

Weather Bureau Technical Notes

TN 33
EDS 1   Part 1: Weather and Disease. H. E. Landsberg. Part 2: Solar Radiation and Skin Cancer Deaths. G. D. Brinckerhoff. February 1966. (PB-169-813)

TN 43
EDS 2   A Bibliography of Meso- and Micro-Environmental Instrumentation. John F. Griffiths and M. Joan Griffiths, July 1966. (PB-173-088)

ESSA Technical Memorandums

EDSTM 3   Climatological Aspects of Air Pollution in West Virginia. Robert O. Weedfall, January 1967. (PB-176-905)

EDSTM 4   Estimates of Winds at Constant Heights Generated From Winds Observed at Constant Pressure Surfaces. H. L. Crutcher, H. B. Harshbarger, R. L. Durham, F. T. Quinlan, J. D. Matthews, and W. B. Tschiffely, February 1967. (PB-174-499)

EDSTM 5   Synoptic Aspects of Mortality: A Case Study. Dennis M. Driscoll, February 1967. (PB-174-500)

EDSTM 6   A Technique for Determination of a Climatology of High Altitude Balloon Trajectories. Frank T. Quinlan and Lee R. Hoxit. October 1968. (PB-180-200)

EDSTM 7   Minimum Temperature Patterns Over New York State on Two Winter Nights. A. Boyd Pack, February 1969. (PB-183-398)

EDSTM 8   Coastal Weather and Marine Data Summary for Gulf of Alaska, Cape Spencer Westward to Kodiak Island. Harold W. Searby, May 1969. (PB-184-784)

EDSTM 9   A Bibliography of Weather and Architecture. John F. Griffiths and M. Joan Griffiths, April 1969. (PB-184-969)

EDSTM 10 A Note on Climatology of Thailand and Southeast Asia. H. L. Crutcher, S. Bintasant Nash, and D. K. Kropp, May 1969. (PB-187-569)

EDSTM 11 Meteorological Drought in West Virginia. Robert O. Weedfall, September 1969. (PB-187-474)

EDSTM 12 Snowfall, Snowfall Frequencies, and Snow Cover Data for New England. R. E. Lautzenheiser, December 1969. (PB-194-221)

EDSTM 13 Applications of Air Mass Classifications to West Virginia Climatology. Robert O. Weedfall, January 1970. (PB-191-966)

EDSTM 14 Georgia Tropical Cyclones and Their Effect on the State. Horace S. Carter, January 1970. (PB-190-768)

GATE RADAR CAPPI DERIVATION FOR THREE-DIMENSIONAL REFLECTIVITY ANALYSES

Peter J. Pytlowany, Frank P. Richards, and Michael D. Hudlow

Washington, D.C.
July 1979

CONTENTS

CONTENTS (Con.)

FIGURES

TABLES

LIST OF SYMBOLS

Symbol	Meaning	Units
A	two-way attenuation due to both molecular oxygen and water vapor	dBZ
A_{H_2O}	one-way attenuation due to water vapor	dB
A_{O_2}	one-way attenuation due to molecular oxygen	dB
n	index of refraction	None
P	atmospheric pressure	atmospheres
R	rainfall rate	mm hr^{-1}
R'	"equivalent" Earth radius	m
R_E	mean radius of the Earth	m
r	slant range	km
s	distance along the Earth's surface	m
w	sine of the elevation angle $(\sin \phi)$	None
Z_e	equivalent reflectivity factor	mm^6 m^{-3}
z	height above the Earth's surface	m
z_o	height of radar antenna above the Earth's surface	m
γ_{H_2O}	attenuation coefficient for water vapor	dB km^{-1}
γ_{O_2}	attenuation coefficient for molecular oxygen	dB km^{-1}
ϕ	radar elevation angle	deg
ρ_w	absolute humidity	gm m^{-3}
θ	radar azimuth angle	deg

Notes:

1) An overbar indicates a vertically averaged value.

2) A subscript of k refers to a variable associated with a discrete CAPPI level (height).

3) A subscript of m refers to a variable associated with a discrete CAPPI range.

GATE RADAR CAPPI DERIVATION FOR THREE-DIMENSIONAL REFLECTIVITY ANALYSES

Peter J. Pytlowany, Frank P. Richards, and Michael D. Hudlow

Center for Environmental Assessment Services[1]
Environmental Data and Information Service, NOAA, Washington, D.C.

ABSTRACT. Methodology and processing techniques used in deriving constant-altitude, plan-position-indicator (CAPPI) arrays of mean reflectivities from GATE Oceanographer radar tilt-sequence data are presented. Input data adjustments and corrections are specified and basic assumptions and motivations relating to particular decisions are discussed. The defining equations and algorithms applied in generating CAPPI arrays are developed for a mean GATE atmosphere. A description of the techniques and mechanics of producing polar coordinate CAPPI arrays and subsequently rectifying them to Cartesian data arrays is given. Computer aspects are discussed and performance results are summarized. The nature and applicability of the CAPPI data sets in scientific investigations define the limits within which quantitative use is meaningful and productive. Data problems and limitations are discussed, and an assessment of data quality and potential sources of error is given to aid in characterizing the qualitative and quantitative aspects of the data. Finally, avenues of potential research applications are broadly categorized and outlined.

1. INTRODUCTION

The GARP[2] Atlantic Tropical Experiment (GATE) was designed to investigate the interactions between meteorological phenomena on different scales in an effort to develop parameterization techniques for cumulus convection in global atmospheric models. Understanding the organization of convection on the cloud-cluster and mesoscales (B and C scales) and its relationship to cloud-scale (D-scale) parameters were primary objectives in the GATE Convection Subprogram.

Quantitative radar data, collected and digitally recorded by systems aboard four of the GATE B-scale ships, provide detailed three-dimensional spatial and temporal coverage of the rainfall patterns and parameters associated with moist convection in the Eastern Atlantic during the summer of 1974.

---

[1]/Formerly the Center for Experiment Design and Data Analysis.
[2]/Global Atmospheric Research Program.

Since the natural radar coordinate system is quasi-spherical, it is inconvenient for analysis techniques based on uniform spacing in the vertical. CAPPI data eliminate this difficulty and facilitate the determination of the structures and lifecycles of convective systems.

The CAPPI reflectivity fields delineated here are comprised of integral estimates of equivalent reflectivity factor[3] (dBZ) having an intensity resolution of 1 dBZ. A set of CAPPI data for a given time is composed of either eight or twelve 64 x 64 Cartesian arrays (scans) spaced at discrete ascending heights. The temporal and horizontal resolutions are 15 min and 4 km, respectively, and no data bin centers extend beyond 126 km from the radar. Only Oceanographer radar data for selected days from all three field Phases of GATE were processed. The selection was based on the presence of significant and interesting meteorological activity, and each selected day covered a period of 24 hr or less and occasionally spanned 2 calendar days. Except for the two lowest heights at 1.5 and 2.0 km, the normal vertical separation between CAPPI levels [4] is 1 km.

The digital tilt-sequence data set collected with the C-band radar system aboard the NOAA ship Oceanographer was used as input in generating the CAPPI data. For Phases I and II, the Oceanographer was stationed at the center of the B-scale hexagon, while its Phase III location was the southeastern corner (position 4 in fig. 1). Normally, data were collected every 15 min at 12 ascending elevation-angle settings. The elevation-angle increment was approximately 2°, but a smaller interval was used between the two lowest elevation angles. The nominal elevation-angle settings for the Oceanographer radar are given in figure 2. At each setting, a full azimuthal polar scan of 360° was automatically recorded. Within the total tilt set, particular scans were occasionally missing due to hardware problems or were eliminated in editing because of severe data problems or the absence of echo content. Therefore, the actual number of

---

3/The terms reflectivity factor and reflectivity are used interchangeably in this report.
4/Although CAPPI "levels" are referred to in this paper, the CAPPI bins (elements) should be considered as estimates over a three-dimensional volume of atmosphere having a depth nominally centered at the CAPPI height.
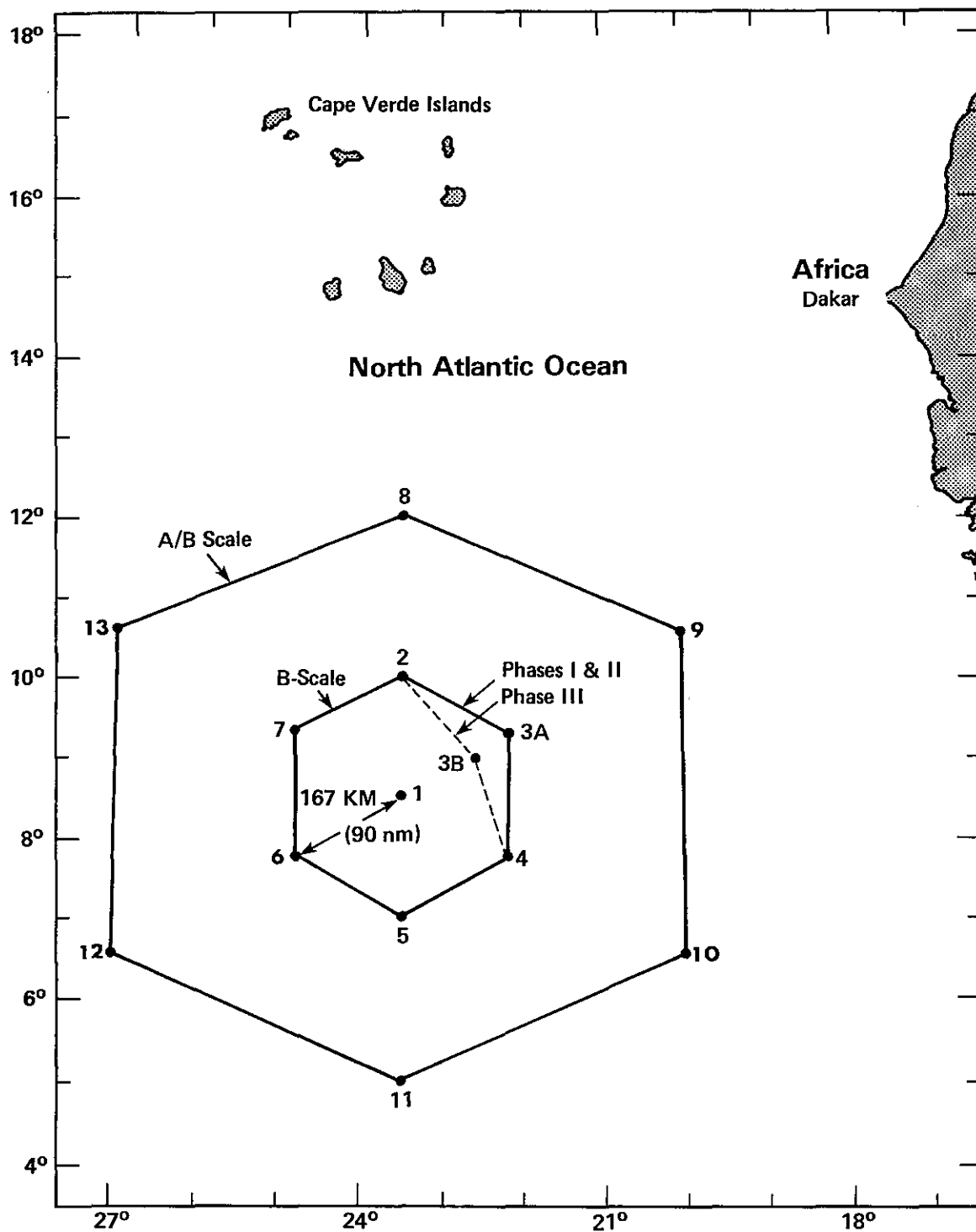
Figure 1.—Ship arrays for GATE (Summer/1974).
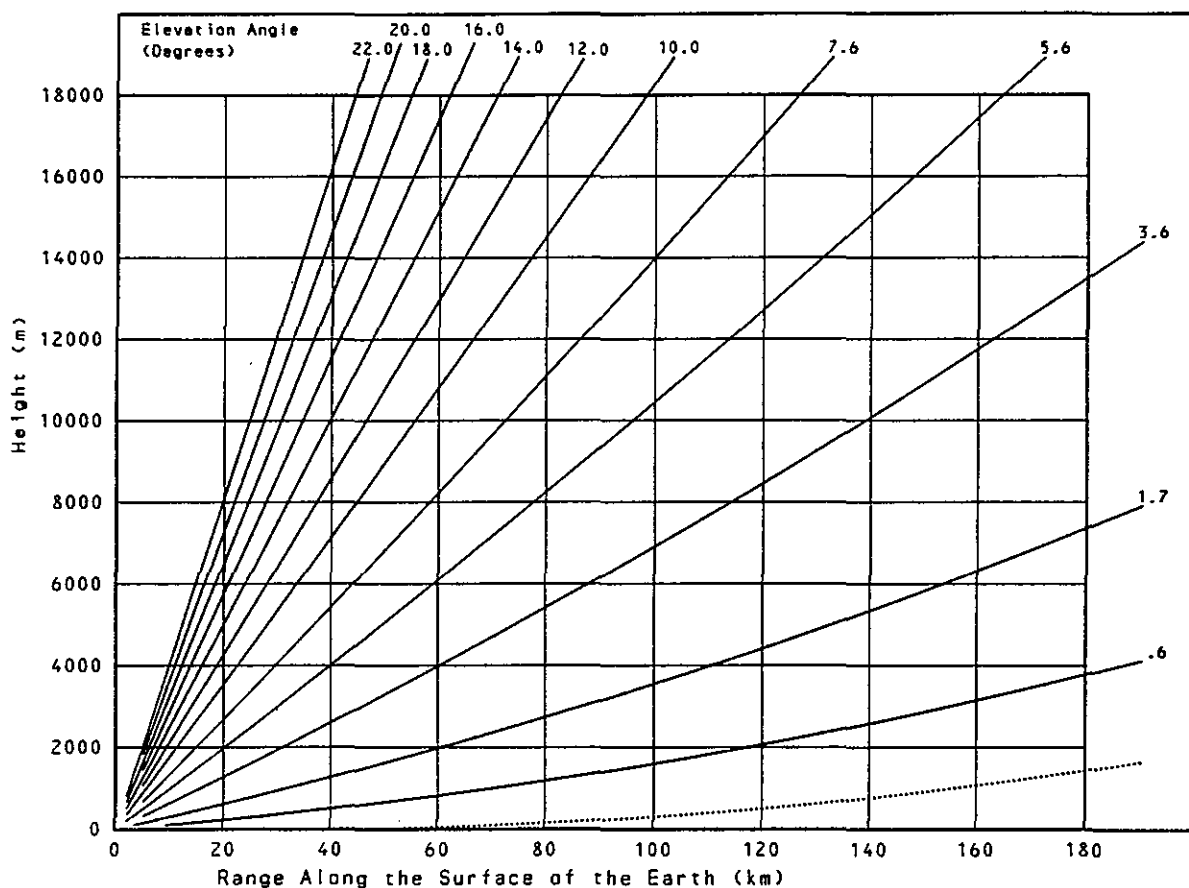
Figure 2.—Beam height versus Earth range for the nominal <u>Oceanographer</u>
antenna tilt angles.

scans available to generate CAPPI arrays could vary from sequence to
sequence.

The derived CAPPI data furnish a relatively comprehensive and detailed
three-dimensional characterization of tropical convection for selected
days during GATE. However, to effectively and prudently use the data
for scientific study and analysis, an adequate understanding of the
motivations and assumptions considered in their derivation is essential.
The techniques, limitations, and quality assessments presented in subsequent
sections should be valuable for potential users.

The methodologies used here may have applicability elsewhere, and
some suggestions are presented in the final section as being promising
areas for analyses based on the CAPPI data. The data are available, both
in microfilm graphic format and on magnetic tapes, from the National

Table 1.—Inventory of the derived Oceanographer radar CAPPI data

Set No.	No. of CAPPI arrays	Phase	Time interval Julian day & GMT
1	1124	I	183/0017–183/2359
2	1152	I	188/0015–189/0000
3	1156	I	194/0900–195/0900
4	1164	II	209/0000–210/0000
5	996	II	221/1500–222/1200
6	952	II	223/2358–224/1958
7	1132	III	245/0015–246/0000
8	1132	III	247/0015–248/0000
9	1148	III	249/0015–250/0000

Climatic Center (NCC) located in Asheville, N.C. (table 1). They may be ordered using the GATE Data Catalogue (World Data Center – A, 1978).

2. DESCRIPTION OF INPUT AND OUTPUT DATA SETS

2.1 Tilt–Sequence Reflectivity Data (Input)

At 15–min intervals throughout the three observational Phases of GATE, three-dimensional radar data were digitally processed and recorded by the Oceanographer's 5.3–cm, C–band system (Hudlow 1975). The circular parabolic antenna sampled the tropical atmosphere by sweeping out a series of twelve 360° azimuthal scans. For successive scans, elevation angles were raised 2° between 0° and 22° (nominally). At a scanning rate of 3 rpm, approximately 4 min elapsed during the collection of a tilt sequence of data. A digital video integrator and processor (DVIP) (Sirmans and Doviak 1973) and a magnetic tape recorder were used to create a 256–level binary data set composed of arrays with intensity estimates for 200 range bins and 180 radials. The spatial resolution is 2 km (slant range) x 2° (azimuth).

The resultant raw data were preprocessed, edited, merged, and converted from engineering DVIP units to meteorological equivalent reflectivity factors (Hudlow 1976a and b and Hudlow et al. 1976) having an intensity resolution of 1 dBZ. The reflectivity estimates were retained for a maximum range of 260 km. If no echo content was discerned in the higher elevation scans, or if severe data problems occurred, the absence or elimination of these scans resulted in validated tilt sequences of varying length.

2.2 Constant-Altitude Reflectivity Data (Output)

The derived CAPPI data are similar to the digitized hybrid reflectivity data (Hudlow 1976b), which can be regarded as a low-altitude, quasi-CAPPI set. For every 15-min tilt sequence, only the lowest three scans were used in constructing the polar hybrids, whereas all available elevation angles were used in generating the 8 or 12 discrete CAPPI arrays. Twelve height arrays were derived if at least the lowest four elevation angles were present; otherwise, the first eight levels were constructed when only the lowest two or three elevation angles existed (fig. 2). Except for the separation between the two lowest levels at 1.5 and 2.0 km, the interval between CAPPI arrays is 1 km.

The 64 x 64 Cartesian arrays contain mean equivalent reflectivity factors, rounded to the nearest integer in the range 0 to 64, providing an intensity resolution of 1 dBZ. These estimates were derived for distances up to 126 km from the radar, and each bin represents the mean reflectivity over an "Earth" area covering 4 km x 4 km at the indicated height.

3. TRANSFORMATIONS AND CORRECTIONS

3.1 The Z-R Relationship

Whenever the CAPPI algorithms involved averaging or interpolation, the reflectivities were converted to rainfall rate units using

$$Z_e = 232 \ R^{1.25} \ , \tag{1}$$

where Z_e is the equivalent reflectivity factor in $mm^6 \ m^{-3}$ [$Z_e = 10^{(dBZ/10)}$] and R is the rainfall rate in $mm \ hr^{-1}$ (Austin et al. 1976). After

6

computations, the resultant rainfall values were then converted back to the nearest integral dBZ.

Although eq. (1) was derived from GATE disdrometer drop-size data collected below the melting level, it was assumed that the exponent in this equation, or a similar one relating Z_e to the liquid water content, did not alter appreciably above the melting layer. Values derived from the interpolation and averaging steps described in section 4 are invariant to changes in the multiplicative coefficient in eq. (1). Since the derivation of equivalent reflectivity factors (dBZ) is relatively insensitive to the potential variability in the Z-R relationship, the assumptions implicit in a universal application of eq. (1) were considered reasonable and appropriate for purposes of CAPPI array generation. For the precipitation analysis, however, variability in the Z-R relationship can affect the accuracy of the rainfall rates (Hudlow and Arkell 1978).

3.2 Systematic Bias Adjustment

The determination and elimination of any bias in the input tilt-sequence data set was an important first step in refining the reflectivity estimates. After a comprehensive and multifaceted intercomparison study, the _Oceanographer_ estimates were found to be low by 2.75 dBZ across the dynamic range. This result was based on analysis of data from all four GATE quantitative radars together with point estimates of precipitation collected by rain gages (Hudlow et al. 1979). A systematic + 2.75-dBZ bias adjustment of all nonzero values was incorporated in a look-up table that used eq. (1) to derive rainfall rates corresponding to the dBZ input data.

3.3 Atmospheric Attenuation Correction

Another significant and constantly present source of intensity degradation results from attenuation of the radar signal by atmospheric gases (Hudlow et al. 1979). Although normally insignificant for the C-band radars during GATE, attenuation during rainfall periods from water-film buildup on the radome or from intervening rainfall can (occasionally) seriously degrade the magnitudes of the radar measurements. The application and subsequent interpretation of rainfall attenuation corrections in CAPPI

analyses were considered impractical for geometrical and economic reasons. Consequently, only the corrections for the atmospheric attenuation effects of diatomic oxygen and water vapor, functionally dependent on slant range and antenna elevation angle, were applied. The GATE normalized equations for attenuation by oxygen and water vapor, respectively, are

$$A_{O_2} = \int_0^r (\gamma_{O_2})\ dr \simeq \int_0^r (0.0075)\ P^2\ dr \tag{2}$$

and

$$A_{H_2O} = \int_0^r (\gamma_{H_2O})\ dr \simeq \int_0^r (0.00028)\ \rho_w\ P\ dr\ , \tag{3}$$

where A_{O_2} and A_{H_2O} are one-way attenuations (dB) to a point at a slant range of r (km), P is pressure in atmospheres, and ρ_w is the absolute humidity of the air (gm/m^3) (Hudlow et al. 1979).

A least-squares quadratic fit to data from a mean GATE sounding between the surface and 200 mb yielded

$$P = 0.993 - 1.057 \times 10^{-4}\ z + 3.395 \times 10^{-9}\ z^2\ , \tag{4}$$

where z is the height above the Earth's surface (m). Fitting the absolute humidity in a least-squares sense, from the surface to 150 mb, required a fourth-degree polynomial expression given by

$$\rho_w = 20.74\ - 7.089 \times 10^{-3}\ z + 9.571 \times 10^{-7}\ z^2 \tag{5}$$
$$- 5.973 \times 10^{-11}\ z^3 + 1.428 \times 10^{-15}\ z^4$$

To enable an analytic integration of eqs. (2) and (3) and to establish the elevation-angle dependency in the final solution, the height of the radar beam above the surface of the Earth was determined with reasonable accuracy by

$$z = 0.059\ r^2 + 1000\ r\ \sin\ (\phi)\ , \tag{6}$$

where ϕ is the elevation angle. Substitution of eq. (6) in eqs. (4) and

(5) and subsequent integration according to eqs. (2) and (3) yielded polynomials in r and sin (ϕ) of high order. A sensitivity analysis for selected slant ranges and tilts allowed elimination of some of the higher order terms and resulted in the following equations:

$$
\begin{aligned}
A_{O_2} \simeq\ & 7.395 \times 10^{-3}\, r - 7.872 \times 10^{-4}\, w\, r^2 \\
& + (4.479 \times 10^{-5}\, w^2 - 3.096 \times 10^{-8})\, r^3 \\
& - (1.346 \times 10^{-6}\, w^3 - 3.963 \times 10^{-9}\, w)\, r^4
\end{aligned}
\tag{7}
$$

and

$$
\begin{aligned}
A_{H_2O} \simeq\ & 2.8 \times 10^{-4}\, \{20.59\, r - 4.616\, w\, r^2 \\
& + (0.590\, w^2 - 1.816 \times 10^{-4})\, r^3 \\
& - (4.615 \times 10^{-2}\, w^3 - 5.240 \times 10^{-5}\, w)\, r^4 \\
& + (2.196 \times 10^{-3}\, w^4 - 6.532 \times 10^{-6}\, w^2 + 1.184 \times 10^{-9})\, r^5 \\
& - (5.895 \times 10^{-5}\, w^5 - 4.318 \times 10^{-7}\, w^3 + 3.072 \times 10^{-10}\, w)\, r^6\} \quad ,
\end{aligned}
\tag{8}
$$

so that

$$
A = 2\,(A_{O_2} + A_{H_2O}) \quad , \tag{9}
$$

where $w = \sin(\phi)$ and A is the total two-way attenuation correction applied (dBZ). The atmospheric attenuation corrections were determined for a set of ranges at each elevation setting within the tilt-sequence up to a maximum $\phi = 8.0°$. At higher tilts, the contribution was less than 0.5 dBZ and, in rounding to the nearest integer, these corrections became zero-valued. The integer dBZ values, corrected for atmospheric attenuation effects, were used to reference tabular rainfall rates already containing the systematic bias adjustment (sec. 3.2).

4. CAPPI DERIVATION

Because a three-dimensional Cartesian coordinate system is more convenient for meteorological and hydrological analyses over limited areas, the radar tilt sequences in spherical coordinates were transformed to CAPPI arrays. Atmospheric refraction, which causes radar beam curvature, and the curvature of the Earth were significant factors affecting the location of the volumetric centers of the digital reflectivity estimates.

The methodology and algorithms as well as the horizontal resolution and vertical separation interval were selected to preserve the structural detail of the tropical convection as revealed in the tilt-sequence input data.

4.1   Radar Beam Geometry

The vertical gradient of the refractive index depends on the pressure, temperature, and water vapor content of the atmosphere. With increasing range and height, the radar beam normally bends slightly toward the Earth as it ascends due to the lapse of humidity and temperature. For mean GATE conditions, a least-squares exponential fit yielded an index of refraction

$$n = 1 + 3.61 \times 10^{-4} \, e^{(-1.4 \times 10^{-4} z)} \tag{10}$$

and a vertical gradient (m^{-1})

$$\frac{dn}{dz} = -5.05 \times 10^{-8} \, e^{(-1.4 \times 10^{-4} z)} \quad . \tag{11}$$

The path of the beam is determined by

$$\frac{d^2 z}{ds^2} - \left(\frac{2}{R_E + z} + \frac{1}{n}\frac{dn}{dz} \right) \left(\frac{dz}{ds} \right)^2 = \left(\frac{R_E + z}{R_E} \right)^2 \left(\frac{1}{R_E + z} + \frac{1}{n}\frac{dn}{dz} \right) \quad , \tag{12}$$

where s and R_E are the distance projected along the Earth and the mean radius of the Earth, respectively. The maximum elevation angle of the Oceanographer tilt-sequence data set was sufficiently small so that

$$\left(\frac{dz}{ds} \right)^2 = \tan^2 \phi < 0.2 \ll 1 \quad .$$

Since n is nearly 1 and $z \ll R_E$, eq. (12) can be approximated with good accuracy by

$$\frac{d^2 z}{ds^2} = \frac{1}{R_E} + \frac{dn}{dz} \quad . \tag{13}$$

For simplicity, replacing the mean Earth radius, R_E, by an equivalent Earth radius, R', enables treatment of ray paths as straight lines relative to the surface of the Earth. An equation for R' in terms of R_E and the gradient of refractive index, dn/dz, is derivable through the use of Snell's

law in spherical geometry (Skolnik 1962). Hence, substituting

$$R' = \frac{R_E}{1 + R_E \frac{dn}{dz}}$$ (14)

in eq. (13) yields (Greene, 1971)

$$\frac{d^2 z}{ds^2} = \frac{1}{R_E} \left(1 + R_E \frac{dn}{dz} \right) = \frac{1}{R'} \quad .$$ (15)

4.1.1 Introduction of a Mean Gradient of Refractive Index

For each atmospheric layer extending from the antenna height above mean sea level, z_o, to a given CAPPI height, z_k, the vertical gradient of refractive index, dn/dz, was replaced by a mean gradient for the whole layer,

$$\overline{\frac{dn}{dz}} (z_k) = \frac{1}{z_k - z_o} \int_{z_o}^{z_k} \frac{dn}{dz} \, dz \quad .$$ (16)

Substituting eq. (11) in eq. (16) gives

$$\overline{\frac{dn}{dz}} (z_k) = \frac{3.61 \times 10^{-4} [e^{(-1.4 \times 10^{-4} z_k)} - e^{(-1.4 \times 10^{-4} z_o)}]}{z_k - z_o} \quad .$$ (17)

Approximating the antenna height as $z_o = 0$ and substituting eq. (17) in eq. (14) gives

$$\overline{R}' (z_k) = \frac{R_E z_k}{z_k - 3.61 \times 10^{-4} R_E [1 - e^{(-1.4 \times 10^{-4} z_k)}]} \quad ,$$ (18)

where $\overline{R}'(z_k)$ is the mean equivalent Earth radius derived and held constant for each CAPPI level, z_k.

Integrating eq. (15) twice and applying the initial conditions at $s = 0$, $dz/ds = \tan (\phi)$, and $z = 0$ gives

$$\frac{dz}{ds} = \frac{s}{\overline{R}'} + \tan (\phi)$$ (19)

and

$$z = \frac{s^2}{2\overline{R}'} + s \tan (\phi) \quad .$$ (20)

11

4.1.2 Polar Coordinate CAPPI Array Generation

The data from a sequence of tilt scans at constant azimuths (Θ) are stacked in vertical planes. Consequently, the geometry is invariant in azimuth. Solving eq. (20) for ϕ gives

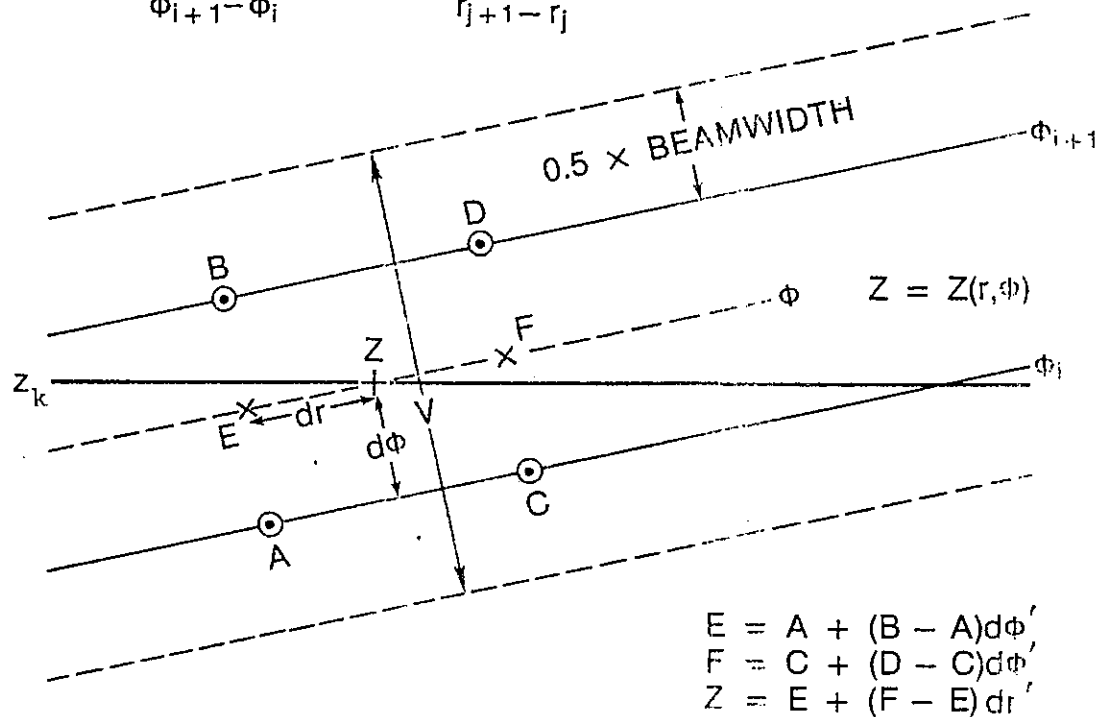$$\phi = \tan^{-1}\left(\frac{z}{s} - \frac{s}{2\overline{R}'}\right) \tag{21}$$

By selecting a set of CAPPI levels $\left\{z_k\right\}$, a corresponding set of equivalent Earth radii $\left\{\overline{R}'_k\right\}$ were computed from eq. (18). For all vertical planes, and at each CAPPI level, z_k, s was varied to create a discrete set of CAPPI range bins $\left\{s_m\right\}$. Using eq. (21), the equivalent antenna elevation settings $\left\{\phi_{(k,m)}\right\}$ from which the radar beam would emanate to intersect a CAPPI level, z_k, at an Earth distance, s_m, were determined. Since the substitution of an equivalent Earth radius enables a linear treatment of ray paths, and since the Earth path for ranges within 130 km can be treated approximately as a straight line, the set of slant ranges $\left\{r_{(k,m)}\right\}$ corresponding to the $\left\{\phi_{(k,m)}\right\}$ were computed as

$$r_{(k,\ m)} = \left(s_m^{\ 2} + z_k^{\ 2}\right)^{\frac{1}{2}} \ . \tag{22}$$

Each polar CAPPI bin, $[r_{(k,m)}, \Theta, \phi_{(k,m)}]$, at height z_k, for which a reflectivity value is derivable, is surrounded by four tilt-sequence input data bins in the same vertical plane. The computation of reflectivity estimates consisted of a bilinear interpolation along <u>elevation angle</u> and <u>slant range</u> coordinate directions (fig. 3). The input reflectivity data were converted to rainfall rate units (sec. 3.1) prior to the interpolation.

In developing the CAPPI procedure, the problem of deteriorating vertical resolution at the farther ranges became apparent, especially in the upper heights. This problem led to nonzero interpolated reflectivities at CAPPI levels above the level at which echo tops were discerned in the tilt-sequence data. As a result, further studies revealed that the bilinear interpolation procedure needed modification to decrease the overshoot. The refinement consisted of inserting a zero value in those cases where (1) both range bins along the higher tilt settings were 0 dBZ (B, D = 0 in fig. 3) and (2) the interpolated CAPPI bin was halfway or closer to these zero bins in an elevation angle sense ($d\phi' \geq 0.5$ in fig. 3).

$$d\phi' = \frac{\phi - \phi_i}{\phi_{i+1} - \phi_i} \qquad dr' = \frac{r - r_j}{r_{j+1} - r_j}$$

$$E = A + (B - A)d\phi'$$
$$F = C + (D - C)d\phi'$$
$$Z = E + (F - E)dr'$$

A,B,C,D — Bin-centered rainfall rate estimates from tilt-sequence data.

V — Thickness of atmosphere represented by CAPPI value Z.

Figure 3.--Geometry used in refined bilinear interpolation procedure to derive a polar CAPPI value, Z, for level, z_k.

## 4.2 Rectification of Polar CAPPI Data

By deriving polar coordinate CAPPI data and converting to Cartesian arrays in separate steps, certain advantages were gained. Both data sets were retained and could be analyzed separately, design and checkout were simplified, and compatibility with the Cartesian hybrid data sets was achieved.

The preservation of hydrologic content in the lower CAPPI levels was considered an important goal. To obtain data useful in a quantitative as well as a qualitative sense, a scheme was selected which had been successfully used in the generation of Cartesian data from polar hybrids. The procedure consists of averaging for ranges ≤ 110 km and radial linear interpolation for ranges > 110 km. The CAPPI rectification process can be outlined as follows:

a. Ranges ≤ 110 km: Derive a mean reflectivity estimate for a Cartesian bin by averaging the rainfall rates for all polar bins with centers falling within the areal extent of the Cartesian bin.

b. Ranges > 110 km: Derive a mean reflectivity estimate for a Cartesian bin by determining the closest radial and linearly interpolating between the rainfall rates from the two neighboring polar data bins (fig. 4).

The technique has the advantage of retaining the quantitative hydrologic content of the three-dimensional data set at the closer ranges and at the lower CAPPI levels without unduly affecting the echo morphology. The main disadvantage is that the inherent smoothing produces some loss of accuracy in preserving the magnitudes of the peaks and gradients.

Since a 2° polar bin at 110 km is approximately equal in azimuthal width to a 4-km Cartesian bin and polar occupancy is sparse or nonexistent at ranges beyond 110 km, linear interpolation became a natural extension to the averaging process in providing hydrologic continuity in the data. Interpolation was restricted to the radial direction to minimize the azimuthal smear at ranges exceeding 110 km.

14
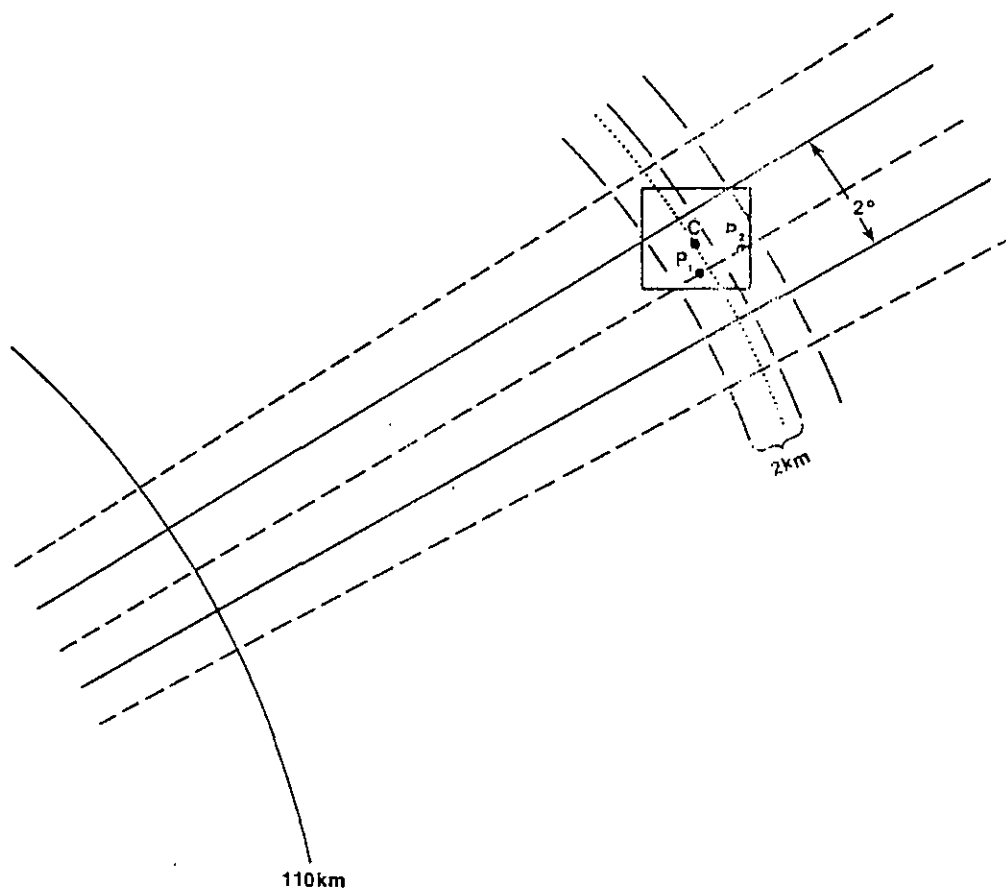
C — Center of Cartesian bin

P₁ P₂ — Centers of polar bins used for interpolation

Figure 4.--Example of polar values that would be used for deriving the estimate for a Cartesian bin at ranges greater than 110 km.

4.3 Computer Considerations

The need to develop flexible processing techniques and software to handle the volume and variability of the input tilt-sequence reflectivity data became apparent in attempting to derive CAPPI arrays in large numbers. The frequency of convective activity during GATE prompted the decision to generate CAPPI data selectively. The times chosen were for periods of 24 hr or less encompassing significant convective events. No more than 1200 CAPPI arrays were derived per processing run, based on a maximum of 12 levels for any 15-min sequence. A total of nine selected days of Oceanographer radar data, three from each Phase of GATE, were processed (table 1).

4.3.1 Software Design Criteria

Since the data volume in the input tilt sequences was substantial, successive generation of 30° sectors (15 radials) for either 8 or 12 levels and storage in a temporary disk file until the complete 360° polar CAPPI arrays were assembled allowed efficient sequential processing while minimizing core requirements. This technique was made possible by the geometrical invariance in azimuth that eliminated the need to track this coordinate. When complete, each CAPPI array was then read from disk and rectified into a Cartesian array.

All polar CAPPI bin locations are uniquely determined by equivalent elevation angles and slant ranges that are invariant relative to the input reflectivity data (sec. 4.1.2). These positional parameters were computed and stored in a look-up table that was referenced to determine incremental distances needed to bilinearly interpolate polar CAPPI estimates (fig. 3). For any given CAPPI bin, only the absolute positions of the four input points varied from sequence to sequence if the particular elevation-angle settings changed. The processing efficiency was greatly enhanced by this technique, since invariant parameters were computed only once.

16

The implementation of the polar-to-Cartesian rectification procedure also employed a table-driven design, which referenced the set of polar coordinates within the Cartesian bins for the averaging procedure and the locations of the input points needed to linearly interpolate along the closest radial at distances exceeding 110 km. Because of symmetry, information for the look-up table was identical in all four quadrants of the Cartesian array, and parameters for only one quadrant were computed and held in core.

4.3.2 Program Performance

Timing tests were conducted on the IBM 360/65 and 360/195 computers. The processing consumed 1.5 min on the IBM 360/65 in creating 12 Cartesian CAPPI arrays with hard copy displays, while only 12 CPU sec were needed on the IBM 360/195. The latter system was used for the CAPPI processing to produce both polar and Cartesian CAPPI tapes and hard copy displays for quality control and monitoring.

5. CAPPI DATA QUALITY AND INTERPRETATION
5.1 CAPPI Data Quality

From the perspective of representing mean reflectivity fields at discrete heights to characterize the vertical structure of the tropical atmosphere, the CAPPI data are of very good quality. There are, however, limitations in interpreting the results and in using the data for deriving various parameters. An attempt was made to be as compatible as possible with other GATE radar data sets while accounting for the inherent differences involved. Intrinsic to the derivation of CAPPI arrays is that input data from the highest elevation angles are used to derive bin estimates at radar-proximate ranges. As a result, contamination due to backscatter

17

from the sea was never apparent in the CAPPI data. Figure 5 provides an
example of the microfilm graphics display for the four lowest CAPPI
arrays at 0000 GMT August 10, 1974.

5.1.1 Consistency of Results

A significant effort was made to define and apply all relevant
corrections and adjustments to the input tilt-sequence data (sec. 3).
Constraints of economy and feasibility precluded corrections for intervening
rainfall attenuation, and the few occasions when significant wet-radome
attenuation occurred were not considered crucial for most CAPPI analyses.
Visual comparison of the microfilm graphics of the four lowest CAPPI
arrays and the hybrid reflectivity data revealed excellent consistency.
Intensity estimates were higher in the CAPPI data, commensurate with the
magnitudes of the input data corrections; structures and cores were
similar and data continuity was notably good.

Prior to the derivation of integrated rainfall fields (Patterson et
al. 1979), a comprehensive intercomparison program had been performed
(Hudlow et al. 1979). Much of the analysis used Cartesian hybrid arrays
from the four C-band radars. The resultant systematic bias adjustments
together with atmospheric attenuation corrections were subsequently
applied to both the instantaneous hybrid and CAPPI fields and led to
excellent agreement between the two (below the melting level). On the
basis of these comparisons, the final CAPPI reflectivity estimates are
probably accurate within a few dBZ.

5.1.2 Specific Problems

A problem of degradation in, and interruption of, data continuity
arose from the obstruction of the radar beam by the superstructure of the
ship. Thus, the accuracy of the reflectivity estimates within a sector
at least 15° wide and centered about the ship's heading was often seriously
degraded, even if the data were not totally obscured. The sector where
measurements were obstructed by the ship's mainmast and stack was estimated
by determining the maximum and the minimum angular extents of all
instantaneous obstructed sectors of all tilts in the sequence and adding
10° to each. Consequently, the unobstructed data region was conservatively
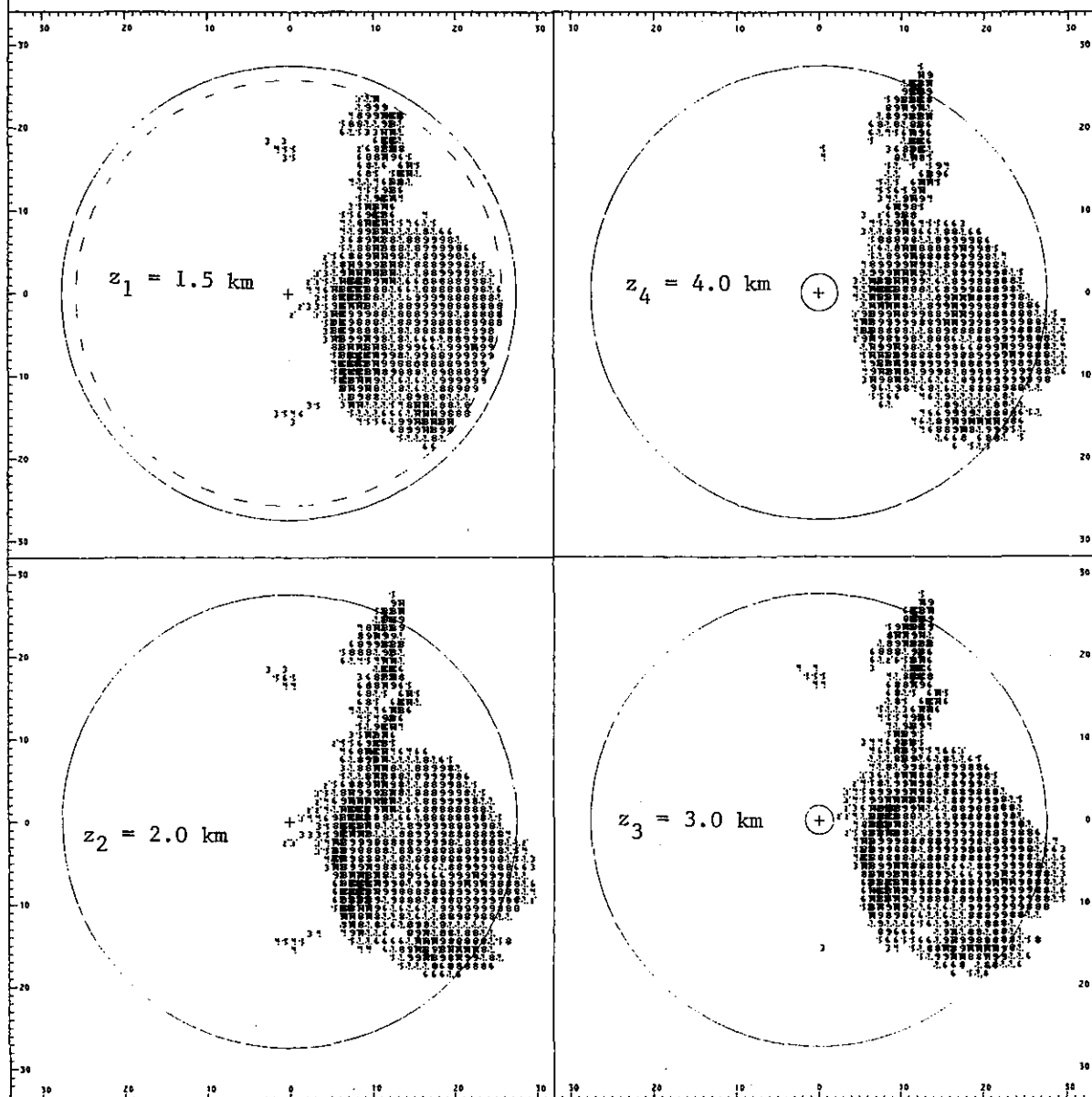
18

Figure 5.--The lowest four CAPPI arrays for 0000 GMT, August 10, 1974.

approximated by taking the obstructed sector to be a wedge 20° wider than the maximum indicated rotation of the ship during the collection of the tilt sequence (fig. 5). The validity of the reflectivities in the "obstructed" region can best be assessed by contextually inspecting the continuity of echo patterns using adjacent times. It is recommended that, when possible, all analyses be restricted to the unobstructed region.

A potentially serious complication in the interpretation of the CAPPI data exists if antenna stabilization inaccuracies exceeded the manufacturer's specifications ($\pm$ 0.5°). Since it is thought that the stabilization errors did occasionally exceed the specifications, this possibility should be considered by anyone attempting to use the data in a quantitative way. For this and other reasons, it may be advisable to reduce the number of CAPPI levels by vertically averaging or by smoothing.

Some effective decrease in vertical and horizontal resolution in the CAPPI data occurred when the corresponding input tilt sequence had a missing base or embedded scan. Cases of a missing base scan or those where the lowest elevation angle exceeded about 0.5° preclude the derivation of the normal CAPPI range bins at the farther ranges, particularly at the 1.5-km level. At times when a sequence lacked an embedded scan, the derivation procedure consisted of using the adjacent tilts having an elevation angle separation interval considerably larger than the nominal 2°. As a result, the normal decrease in resolution with increasing range became much more pronounced (fig. 2).

5.2 Interpretation and Limitations

The primary limitation of the CAPPI data arises from the nature and resolution of the spherical coordinate system associated with the input tilt-sequence data set. Figure 2 is based on nominal elevation angles for the Oceanographer radar and schematically illustrates the relationship between the radar coordinate system and levels above the surface of the Earth. Taking corresponding range bins along any two elevation angles (ϕ_1, ϕ_2), the incremental height displacement (Δz) increases and thus the effective vertical resolution decreases with slant range (r) and with the

20

difference between the two tilt settings such that, to a first approximation,

$$\Delta z = r(\sin\phi_1 - \sin\phi_2)$$

Since the derivation of the polar CAPPI arrays consisted of bilinear interpolation along the <u>slant range</u> and <u>elevation angle</u> coordinate directions, data smearing became greater at the farther ranges as adjacent tilts diverged. As mentioned, the problem was especially magnified whenever an embedded tilt was missing. Consequently, the same four input points may have entered into the bilinear interpolation for corresponding polar CAPPI bin values at successive heights (fig. 3). The vertical structure was then resolved in less detail with increasing range as the elemental sampling volume increased.

Implicit to the use of the radar equation in converting backscattered power to reflectivities is the assumption that the radar beam and sampling volumes were uniformly filled with hydrometeors. Since this assumption weakens with increasing range and sampling volume, beam-filling problems can result in CAPPI reflectivity estimates that are degraded somewhat at the far ranges. Also, the effective radar sensitivity decreases with range, preventing the detection of very weak echoes at the far ranges (Richards and Hudlow 1977).

The CAPPI arrays were derived with a vertical separation interval of 1 km to retain the details of the vertical structure at the closer ranges where this is possible. It is very important to remember that the reflectivity values from the input tilt sequences were not point estimates but, rather, were averages over elemental volumes of 2 km (slant range) x 2° (azimuth) x 1.5° (beamwidth). The coordinates of the center points of the volumes were used in the bilinear interpolation technique to generate the CAPPI data. Therefore, the CAPPI bins are estimates over a three dimensional volume of atmosphere having a depth nominally centered at the CAPPI height. Since the depth interval of the input data bins increases with range, the 1-km increment between CAPPI arrays does not imply that the vertical resolution is that good at the farther ranges. In fact, at ranges exceeding about 100 km, the "effective" resolution in the vertical

is more nearly 4 km. Because of this and other range-dependent effects, data beyond 100 km should be regarded (optimistically) as semiquantitative.

The beginning time in the collection of a given tilt sequence was assigned to all CAPPI arrays generated for that 15-min period. It is important to recognize that the CAPPI reflectivity estimates are not "instantaneous" but represent data spanning an interval as long as 4 min. Consequently, the temporal lag is an important consideration in the interpretation of results from CAPPI analysis characterizing the development and evolution of structural features of convective systems.

A cone, having the vertex at the radar origin and generated by the highest available elevation angle, defines a surface within which no reflectivity estimates are derivable. For a given CAPPI level, z_k, the data-void region is bounded by a circle centered directly above the radar origin, formed by the intersection of the cone with a horizontal plane at height, z_k. The circle increases in radius with increasing z_k, producing a void that becomes significant when considering echo clusters or entities that pass directly over the radar site during their lifecycles. (See "closest derived polar range" in fig. 5.)

In transforming CAPPI reflectivity estimates to hydrologic units, it is important to consider phase changes above the melting level. A Z-R relationship for low-level precipitation estimates will be inappropriate when ice or snow exists, possibly in a mixed state with supercooled water, at levels within and above the melting layer. Caution should be observed in estimating hydrologic content in this region where an alternate to eq. (1) must be sought to relate equivalent liquid-water content to reflectivity.

In summary, it appears that the CAPPI data can be used qualitatively to reveal the structure and internal features of tropical convection. To effectively use the data quantitatively, one must be cognizant of the limitations and exercise care.

6. POTENTIAL RESEARCH APPLICATIONS

Despite limitations and constraints regarding interpretation, the CAPPI data provide a unique three-dimensional characterization of the development, evolution, and spatial structure of convective systems and their component elements during "disturbed" time periods of GATE. The microfilm graphics and digital tape sets are complementary, although each has its own applications. Modeling studies, statistical analyses, and intercomparisons with other systems are simplified by the Cartesian format and the relatively narrow vertical separation interval. Default values and header information delimiting array boundaries, which are described in the documentation accompanying the data sets, facilitate data interpretation and integration in the spatial and temporal domains.

6.1 Structure Studies

Vertical cross sections of reflectivity patterns or range height indicator (RHI) arrays can be constructed directly from the digital CAPPI data along any vertical plane within the 4-km x 4-km grid network. By deriving areal statistics at discrete levels, it is possible to relate CAPPI data with aircraft hydrometeor content measurements, thermodynamic data, etc. The three-dimensional kinematics of the convective environment may be described and the transports of water and heat estimated using existent models.

To examine the correlations between geometrical parameters such as echo size, height, and orientation, echo census methods can be applied either at discrete levels or to the three-dimensional arrays. Other parameters that aid in characterizing convective activity, among them entrainment factors and flux distributions, may be inferred. It is possible to estimate heights of echo tops directly from the CAPPI data. By considering convective entities for suitably restricted range intervals, a reasonably accurate estimate of maximum echo height can be determined up to 12 km. However, an alternate approach is to use the echo-top data set archived on microfilm (Hudlow 1977). (Order from the GATE Data Catalogue, World Data Center - A, 1978.) The echo-top data have the same horizontal

23

resolution as the CAPPI data and provide temporal coverage throughout GATE, but maximum echo heights up to 17 km can be discerned.

A bulk statistical evaluation of the effects of any variation with height in the relationship between reflectivity and hydrometeor content on the calculations for rate-of-change in water storage is feasible using the CAPPI data. The aircraft cloud-physics data should also be helpful in this evaluation. A stratification of the CAPPI arrays for levels above and below the melting layer should aid in assessing the effects of hydrometeor phase changes in relating reflectivity to hydrologic content. Results for meteorologically different time periods within the GATE could be compared and evaluated.

By considering slices through echoes, an analysis of gradient fields can be undertaken. Spatial, spectral techniques could be applied in identifying the features, characteristics, and distributions of cores.

6.2 Lifecycles

Vertically integrated and total volumetric hydrometeor content can be computed, and variations with the development and evolution of convective systems can be studied using time-series analysis. It appears feasible to use CAPPI data to investigate the time change of water storage, which should lead to improvements in the interpretations and accuracy of cloud budget analyses.

Durations of many echo entities or clusters can be determined from the CAPPI data. (Satellite data might be used to extend the coverage for those convective systems that persist outside the radar range.) The growth cycles of systems and their elements could be described in terms of the time-dependent variations of maximum echo height, maximum rain rate, etc.

24

Over their lifetimes, convective systems could be studied to determine the development and evolution of vertical structure. Hydrometeor content for geometric areas or for entities or clusters can be vertically integrated and possibly stratified below and above the melting level. The analysis of the time series of these quantities, or those developed from a finer vertical stratification, could aid in determining the morphological evolution of convection.

In using the CAPPI data to examine the evolution of convective systems, a case study approach is appropriate. Special care is necessary in those instances where quantitative results are sought, such as in modeling studies. Prudent selection of high quality periods, particularly those free of obstructed sector problems, is recommended for statistical analyses.

ACKNOWLEDGMENTS

5/Center for Environmental Assessment Services (CEAS).
6/Environmental Science Information Center (ESIC).

REFERENCES

Austin, P. M., S. G. Geotis, J. B. Cunning, J. L. Thomas, R. I. Sax, and
     J. R. Gillespie, "Raindrop Size Distributions and Z-R Relationships
     for GATE," presented at the 10th Tech. Conf. on Hurricanes and
     Tropical Meteor., Abstract published in the Bull. of the Amer. Meteor.
     Soc., Vol. 57, No. 4, 1976, p. 518.

Greene, Douglas R., "Numerical Techniques for the Analysis of Digital Radar
     Data with Applications to Meteorology and Hydrology," Ph.D. Disserta-
     tion, Texas A&M University, College Sta., Tex., 1971, 125 pp.

Hudlow, Michael D., "Collection and Handling of GATE Shipboard Radar Data,"
     Preprints, 16th Radar Meteor. Conf., Amer. Meteor. Soc., April 1975,
     pp. 186-193.

Hudlow, Michael D., "Documentation for the GATE NOAA Radar Tilt Sequence Data,"
     GATE Processed and Validated Data, GATE World Data Center A, National
     Climatic Center, NOAA, Federal Bldg., Asheville, N.C., 1976a, 34 pp.

Hudlow, Michael D., "Documentation for the GATE NOAA Radar Hybrid Data," GATE
     Processed and Validated Data, GATE World Data Center A, National Climatic
     Center, NOAA, Federal Bldg., Asheville, N.C., 1976b, 31 pp.

Hudlow, Michael D., "Documentation for the GATE NOAA Radar Echo Top Graphics
     Data," GATE Processed and Validated Data, GATE World Data Center A,
     National Climatic Center, NOAA, Federal Bldg., Asheville, N.C., 1977,
     14 pp.

Hudlow, Michael D., Peter J. Pytlowany, and Frank D. Marks, "Objective Analysis
     of GATE Collocated Radar and Rain Gage Data," Preprints, 17th Radar
     Meteor. Conf., Amer. Meteor. Soc., Oct. 1976, pp. 414-421.

Hudlow, Michael D. and R. E. Arkell, "Effect of Temporal and Spatial Sampling
    Errors and Z-R Variability on Accuracy of GATE Radar Rainfall Estimates,"
    Preprints, 18th Conf. on Radar Meteor., Amer. Meteor. Soc., Mar. 1978,
    pp. 342-349.

Hudlow, M., R. Arkell, V. Patterson, P. Pytlowany, F. Richards, and S. Geotis,
    "Calibration and Intercomparison of the GATE C-band Radars," NOAA Tech.
    Report EDIS 31, Center for Environmental Assessment Services, NOAA,
    U.S. Dept. of Commerce, Washington, D.C., (in preparation), 1979.

Patterson, V., M. Hudlow, P. Pytlowany, F. Richards, and J. Hoff, "GATE
    Radar Rainfall Processing System," NOAA Tech. Memo. EDIS 26, Center for
    Environmental Assessment Services, NOAA, U.S. Dept. of Commerce,
    Washington, D.C., 1979, 34 pp.

Richards, Frank and Michael D. Hudlow, "Use and Abuse of the GATE Digital
    Radar Data," 11th Tech. Conf. on Hurricanes and Tropical Meteor.,
    Amer. Meteor. Soc., Dec. 1977, pp. 216-223.

Sirmans, Dale and R. J. Doviak, "Meteorological Radar Signal Intensity Estim-
    ation," NOAA Tech. Memo. ERL NSSL-64, NOAA, U.S. Dept. of Commerce,
    Boulder, Co., 1973, 80 pp.

Skolnik, M. I., Introduction to Radar Systems, McGraw-Hill, New York, 1962,
    648 pp.

World Data Center - A, GATE Data Catalogue, National Climatic Center, NOAA,
    Federal Bldg., Asheville, N.C., 1978, pp. 4.36.02.103, 4.36.02.106,
    and 5.36.02.106.